(Received 8 June 2024, Accepted 15 July 2024, Scheduled 22 July 2024)

A Diamond-Type Broadband Microstrip Patch Antenna with a Folded Floor

Han Lin and Yiwei Tao*

School of Electrical and Information Engineering, Anhui University of Science and Technology, Huainan 232001, China

ABSTRACT: In this paper, a diamond-shaped broadband high-gain microstrip patch antenna based on a folded floor structure is proposed. The overall dimensions of the antenna are 108 mm×100 mm×25 mm. Additionally, it contains a radiating microstrip patch, a folded ground plane, and a capacitive feed strip. The broadening of the antenna's operating band is achieved by enhancing the microstrip radiating patch and capacitive feed band. The original rectangular structure was transformed into a rhombic structure, enabling the radiating patch to absorb the current more effectively and achieve a better impedance match for the antenna operating around 5 GHz. The radiation performance of the antenna is maximized by utilizing the folded floor structure. Measured results show that the impedance bandwidth of the antenna is about 61.5% (2.84 GHz–5.36 GHz), covering 5G dual bands. Meanwhile, the peak gain reaches 12.6 dBi, and the average gain reaches 10.7 dBi.

1. INTRODUCTION

Microstrip patch antennas offer numerous advantages, including small size, light weight, easy integration, various feeding methods, simple installation, and low cost [1, 2]. However, narrow bandwidth and low gain are also shortcomings that cannot be ignored in traditional patch antennas. With the advent of 5G communication technology, the bandwidth and gain requirements for microstrip patch antennas are increasing.

To increase the operating bandwidth of microstrip patch antennas, many excellent methods have been proposed. First of all, increase the thickness of the substrate or use a substrate with a smaller dielectric constant or a larger dielectric loss angle tangent [3–5]. These two methods are straightforward, but the problem to consider is that they can lead to an increase in the size of the antenna or a decrease in the efficiency of the antenna. Secondly, a multilayer structure is used to extend the bandwidth of the antenna [6]. However, the disadvantage is that the matching adjustment is complicated and has low accuracy, and the design is difficult. Third, slots are cut in metal patches or floors to achieve broadband characteristics. For example, a dual U-slot antenna is proposed in [7]. The antenna features a 3.1 GHz operating bandwidth that is 50% greater than the original antenna bandwidth. Finally, attaching a parasitic patch is also a simple and effective method [8, 9]. The above methods increase the bandwidth of a microstrip patch antenna but do not improve the efficiency and gain of the antenna.

A microstrip patch antenna based on a broadband high-gain frequency-selective surface is proposed in [10, 11]. Although the bandwidth and gain of the antenna have increased, the design of the antenna is complex and environmentally demanding. In addition, incorporating slots on the microstrip patch to excite multiple patterns has been shown to increase antenna gain [12, 13]. However, the bandwidth of the antenna [13] is smaller than that of other antennas, and the structure of the antenna [12] is slightly more complicated than other antennas. In [14], a broadband high-gain antenna based on a mushroom-shaped structure is presented. This design introduces a new resonance mode that, when being combined with the original mode, enables the antenna to achieve both broadband coverage and high gain. Recently, various antennas based on folded structures have been proposed to achieve high gain and broadband performance [15, 16]. In [15], a folded strip antenna based on metamaterials is proposed, where the upper part of the antenna consists of folded strips, in order to achieve a high gain for the antenna.

To sum up, a novel broadband high-gain microstrip patch antenna is proposed in this paper, which comprises a diamond-shaped radiating unit and a ground structure folded 90 degrees on both sides. The improved diamond shape of the radiating element improves the impedance matching and resonance pattern to widen the bandwidth of the antenna and increase the peak gain of the antenna. The rest of this paper is organized as follows. Section 2 discusses the design process of the antenna, parametric simulation studies, and the analysis of surface currents. Section 3 discusses the experimental results obtained on the fabricated prototype. Finally, Section 4 concludes this paper.

2. ANTENNA DESIGN

2.1. Antenna Structure Design Analysis

2.1.1. Antenna Structure Design

The proposed antenna is a modification of that in [17–19], which uses a suspended microstrip patch, and also [17] uses

* Corresponding author: Yiwei Tao (2023200722@aust.edu.cn).

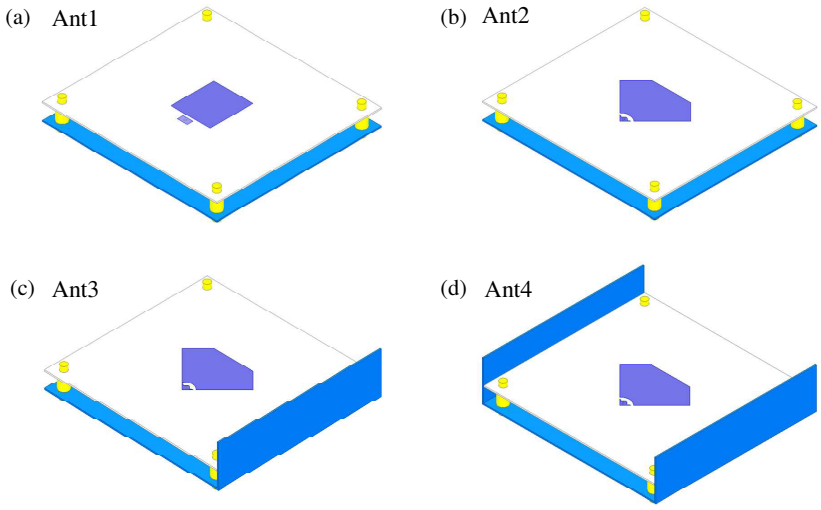

FIGURE 1. The antenna structure design evolution: (a) Ant1, (b) Ant2, (c) Ant3, and (d) Ant4.

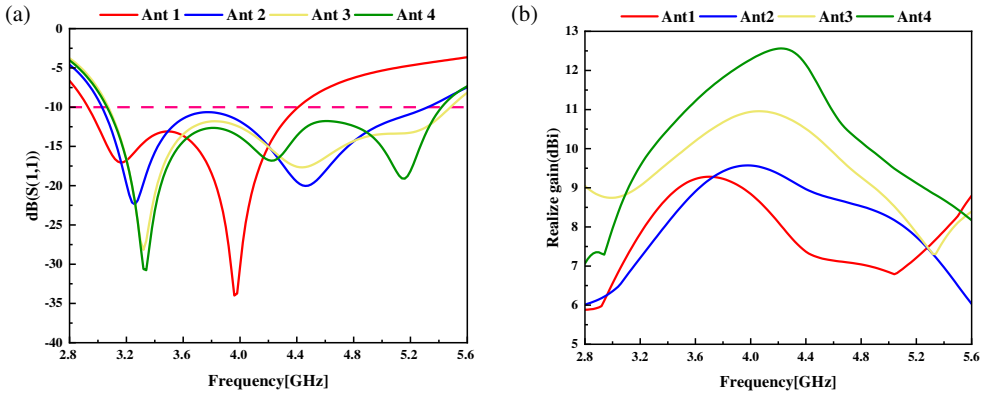

FIGURE 2. Simulation of S-parameters and gain for four antenna structures (a) S_{11} and (b) Gain.

a folded floor structure. The typical height of the suspended substrate (g) above the ground plane is given by [19]

$$g = 0.16\lambda_0 - h\sqrt{\varepsilon_r} \tag{1}$$

where h and ε_r are the thickness and dielectric constant of the substrate, respectively, and λ_0 is the wavelength at the center frequency.

The evolved structure of the antenna is shown in Figure 1. Referring to Figure 1(a), a rectangular capacitive feed strip and a rectangular microstrip patch form the radiating unit. In addition, the radiating unit is printed on a suspended dielectric substrate, and the base plate is connected to the dielectric substrate through a feed line. As shown in Figure 2, the bandwidth of the antenna ranges from 2.93 GHz to 4.41 GHz, and the peak gain reaches 9.28 dBi.

As shown in Figure 1(b), the shapes of the capacitor-fed strip and microstrip patch are altered. Together, the two form a diamond-shaped radiating unit. As shown in Figure 2(a), the improved microstrip patch shifts the low-frequency resonance point slightly to the right and does not improve the impedance matching around the 3 GHz frequency. In addition, the high-frequency resonance point of the antenna is significantly shifted to the right, and the improved high-frequency resonance pattern results in a capacitively reduced impedance around the 5 GHz frequency. The impedance of the antenna is matched, resulting in a widened bandwidth. The bandwidth of the antenna increases from 3.03 GHz to 5.32 GHz, which is 0.81 GHz higher than the bandwidth of antenna 1, and the peak gain reaches 9.57 dBi.

As shown in Figure 1(c), after optimizing the bandwidth of the antenna, the next step is to consider the gain of the antenna. It has been shown in [17] that when the folded floor is parallel to the radiating edge of the patch, the interference currents on the folded floor will somewhat reduce the impedance bandwidth of the antenna as well as not have an increasing effect on the antenna gain. Therefore, one of the non-radiating edges of the patch is folded. Figure 2 (b) shows that the antenna gains increase to 10.9 dBi as expected, and the bandwidth of the antenna is also slightly increased.

This is the final structure of the antenna evolution as shown in Figure 1(d). This time an attempt was made to add a folded floor structure on both sides of the non-radiating edge of the antenna patch. Figures 2(a) and 2(b) show that the antenna bandwidth remains essentially unchanged, and the gain of the antenna is increased to 12.62 dBi.

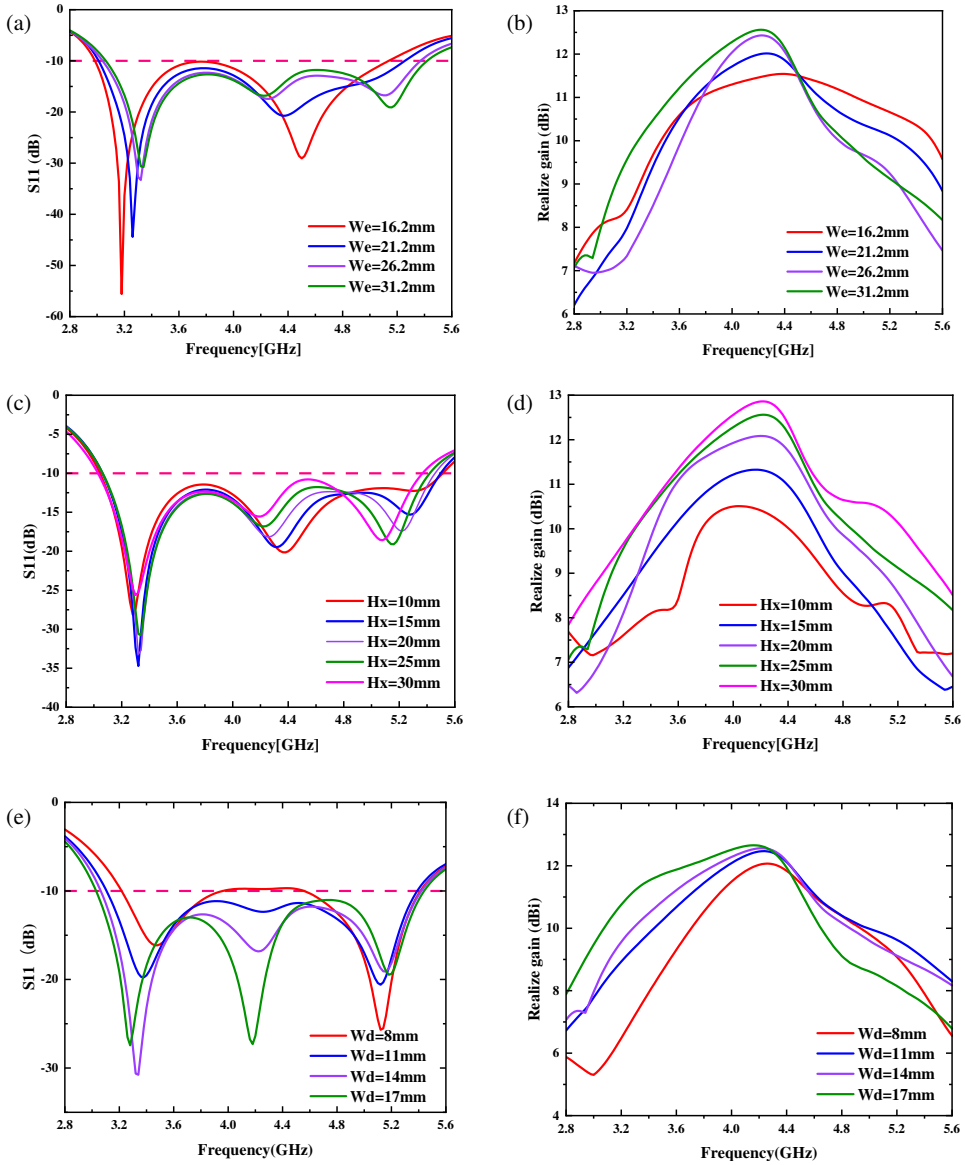

FIGURE 3. The effect of different values of We, Hx and Wd on the reflection coefficient and gain.

In conclusion, the antenna with a folded base has a peak gain 3.3 dBi higher than the antenna without such a structure. After optimization of the radiation unit, the antenna achieves an average gain of 10.76 dBi, and the impedance bandwidth is increased from 40.3% (2.93 GHz–4.41 GHz) to 55.2% (3.07 GHz–5.41 GHz).

2.1.2. Antenna Parameter Analysis

The antenna structure and parameters are simulated and optimized by HFSS during the antenna design process to optimize the performance of the designed high-gain broadband antenna. The optimization process involves optimizing a single parameter while keeping all other parameters constant, and the results of this optimization are displayed in Figure 3. As shown in Figures 3(a) and 3(b), the bandwidth of the antenna increases slightly with the increase of *We*. Although the antenna return loss reaches 55 when the value of *We* is small, the gain of the antenna is significantly low. Since the radiating units of the antenna are at the same distance from the folded floor on both sides for the optimized $We = 31.2$ mm, the reflection coefficient and gain of the antenna will not be significantly improved any further when the value of *We* continues to increase. As shown in Figures 3(c) and 3(d), the impedance bandwidth of the antenna is not significantly affected as the value of Hx increases. The gain of the antenna is gradually increasing when the antenna height is below $Hx = 25$ mm, and there is no significant improvement in the antenna gain when the height of the antenna is above this value. As shown in Figures 3(e) and 3(f), when the patch edge truncation size $Wd = 8$ mm, the S_{11} of some frequencies is higher than -10 dB, and the operating bandwidth of the antenna is significantly narrowed. When the size is increased to 11 mm, the antenna's bandwidth returns to normal and remains unchanged with the increase in size. However, the depth of the S_{11} curve for $Wd = 14$ mm is deeper; the return loss is larger; and the antenna impedance is better

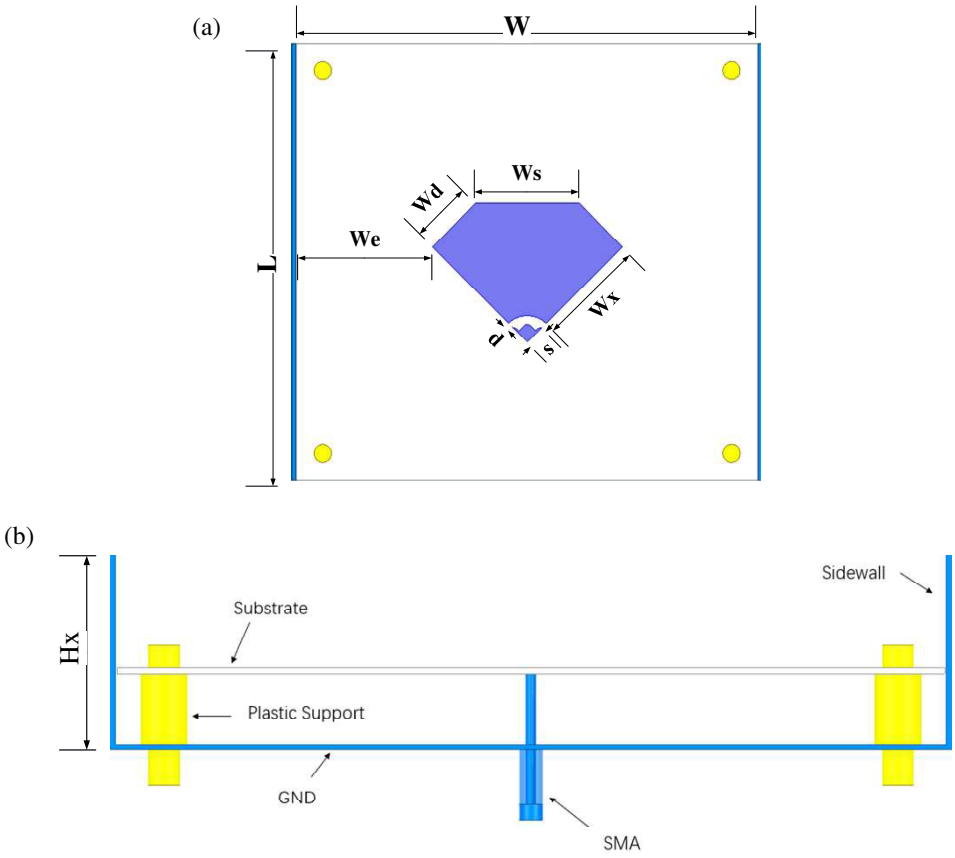

FIGURE 4. Antenna geometry. (a) Top view. (b) Side view.

matched. In addition, the peak gain of the antenna does not change significantly with a gradual increase in the value of Wd, and it is clear that the change in edge size has little effect on the radiation performance. In summary, the optimum result is 31.2 mm for We, 25 mm for Hx, and 14 mm for Wd, which gives the best operating bandwidth as well as gain.

2.2. Final Model of the Antenna

The geometry of the antenna is shown in Figure 4 and consists of three parts: a suspended radiating patch, a copper grounding plate folded on both sides (with dimensions of 108 mm$\times$ 100 mm$\times$25 mm), and four plastic support frames. Diamond patches are printed on the top layer of the dielectric substrate, where the capacitive feeder tape is located next to the radiating patch. The dielectric substrate is made of inexpensive common FR4 material with a thickness of 0.8 mm, a relative permittivity of 4.4, and a loss angle tangent of 0.02. The antenna is coaxially fed. The optimized dimensions of the proposed broadband high-gain antenna are shown in Table 1.

TABLE 1. Optimized dimensional parameters of the proposed antenna.

Parameters	W	L	Ws	Wx	We
Value (mm)	108	100	23.9	24.76	31.2
Parameters	Wd	d	s	Hx	
Value (mm)	14	1.31	4.83	25	

Figure 5 illustrates the equivalent circuit of the designed antenna, where Circuit 1 and Circuit 3 are equivalent to a probe with a feed strip and a suspended diamond-shaped radiating patch. C_4 and C_6 in Circuit 2 denote the end capacitance of the feeder tape and the capacitance at the end of the radiating patch, respectively, and the series capacitance C_5 denotes the gap between them. The size of the radiating patch represented by the parallel resonant circuit consisting of L_{patch}, C_7, and R_2 is corrected to obtain the optimum bandwidth.

2.2.1. Antenna Surface Current Analysis

As shown in Figure 6, the scalar surface current distribution of the antenna at the three resonance points within the operating bandwidth is displayed. It can be seen that the patch current strength at 3.36 GHz is significantly low compared to the other two resonance points. A significant portion of the current at this frequency is concentrated around the floor aperture, making the current not effectively radiate through the metal patch. The current of the antenna is at 4.24 GHz, and the current intensity around the floor aperture is weakened, and the patch current intensity is obviously increased. The resonance mode at this frequency is conducive to improving the radiation performance of the antenna. In addition, the difference between the current at 5.18 GHz and the current at 4.24 GHz is that the distribution of the floor current and its intensity are different.

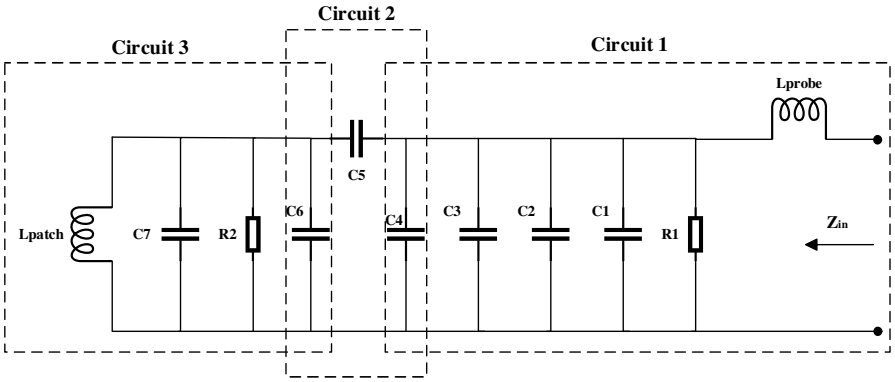

FIGURE 5. Equivalent circuit of the designed high gain broadband antenna.

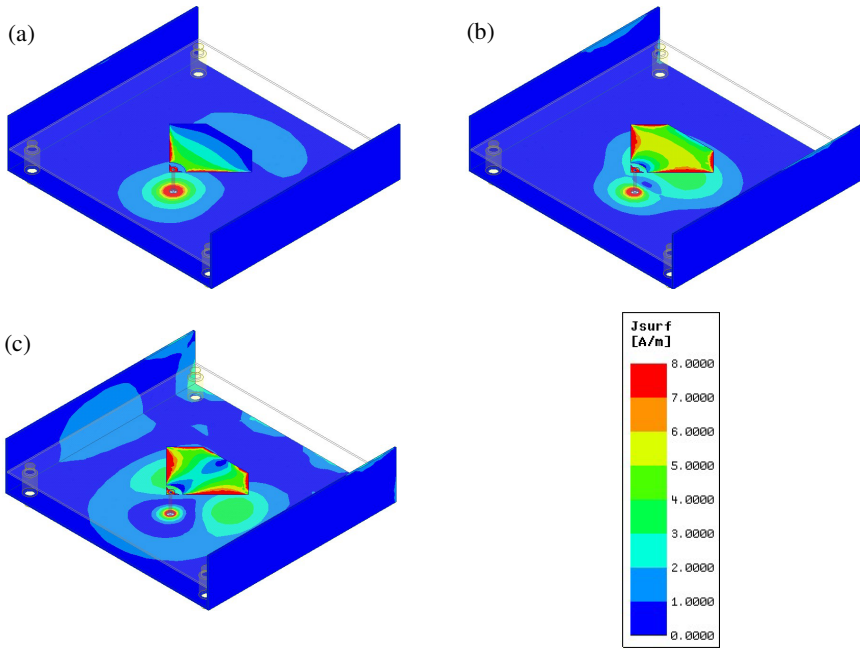

FIGURE 6. S_{11} Scalar surface current distribution for resonant modes in bandwidth. (a) 3.36 GHz, (b) 4.24 GHz, (c) 5.18 GHz.

This causes the antenna to generate a new resonance mode at 5.18 GHz, which improves the impedance matching.

As shown in Figure 7, the surface currents at 5.18 GHz for four different structures of antennas are displayed and further analyzed to show the effect of variations in the radiating cells and the floor on the impedance bandwidth and gain of the antenna. Referring to Figures 7(a) and 7(b), the current intensity on the antenna radiating unit of structure (b) is significantly larger than that in structure (a) under the same excitation. This indicates that the antenna in Figure 7(b) absorbs the current better and obtains better impedance matching. In a previous simulation study, the change in the antenna structure in Figure 7(b) caused the antenna's S_{11} to drop below -10 dB around 5 GHz, which in turn broadened the antenna bandwidth. As shown in Figure 7(c), surface waves on the sidewalls close to the non-radiating edge of the patch generate in-phase currents, and the radiated electric fields generated by these in-phase currents will add up in the boresight direction, thereby contributing to the boresight radiation of the antenna and increasing the antenna gain. As shown in Figure 7(d), the in-phase currents in the two sidewalls of the patch's non-radiating edge are more obvious for enhancing the antenna's radiation performance. Also, the change in the floor structure caused a greater current strength on the radiating unit, causing the antenna to resonate at 5.18 GHz.

3. EXPERIMENTAL SIMULATION AND MEASUREMENT

3.1. S-Parameters

The S-parameters of the antenna are measured using a vector network analyzer of the Agilent N5235A type. The antenna microwave darkroom measurement environment and the prototype manufactured are shown in Figure 8. From the S-parameter curves in Figure 9, the S_{11} measurements of the antenna do not differ much from the simulation results. The measured resonance point is slightly shifted to the left, but the

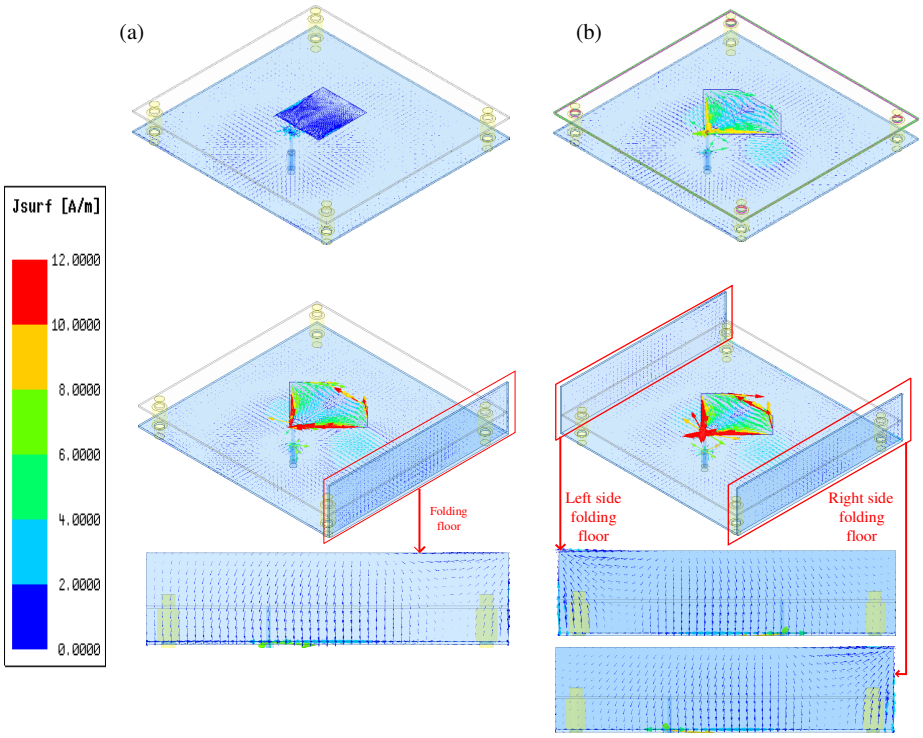

FIGURE 7. 5.18 GHz vector surface current distribution. (a) Ant1, (b) Ant2, (c) Ant3, (d) Ant4.

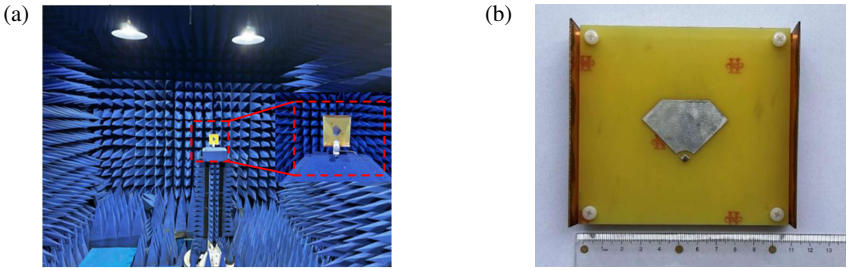

FIGURE 8. The proposed antenna (a) Antenna microwave darkroom measurement environment and (b) fabricated prototype.

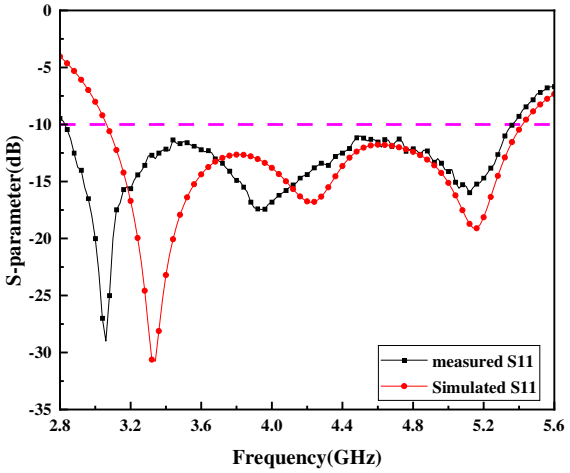

FIGURE 9. Simulated and measured S parameters of the antenna.

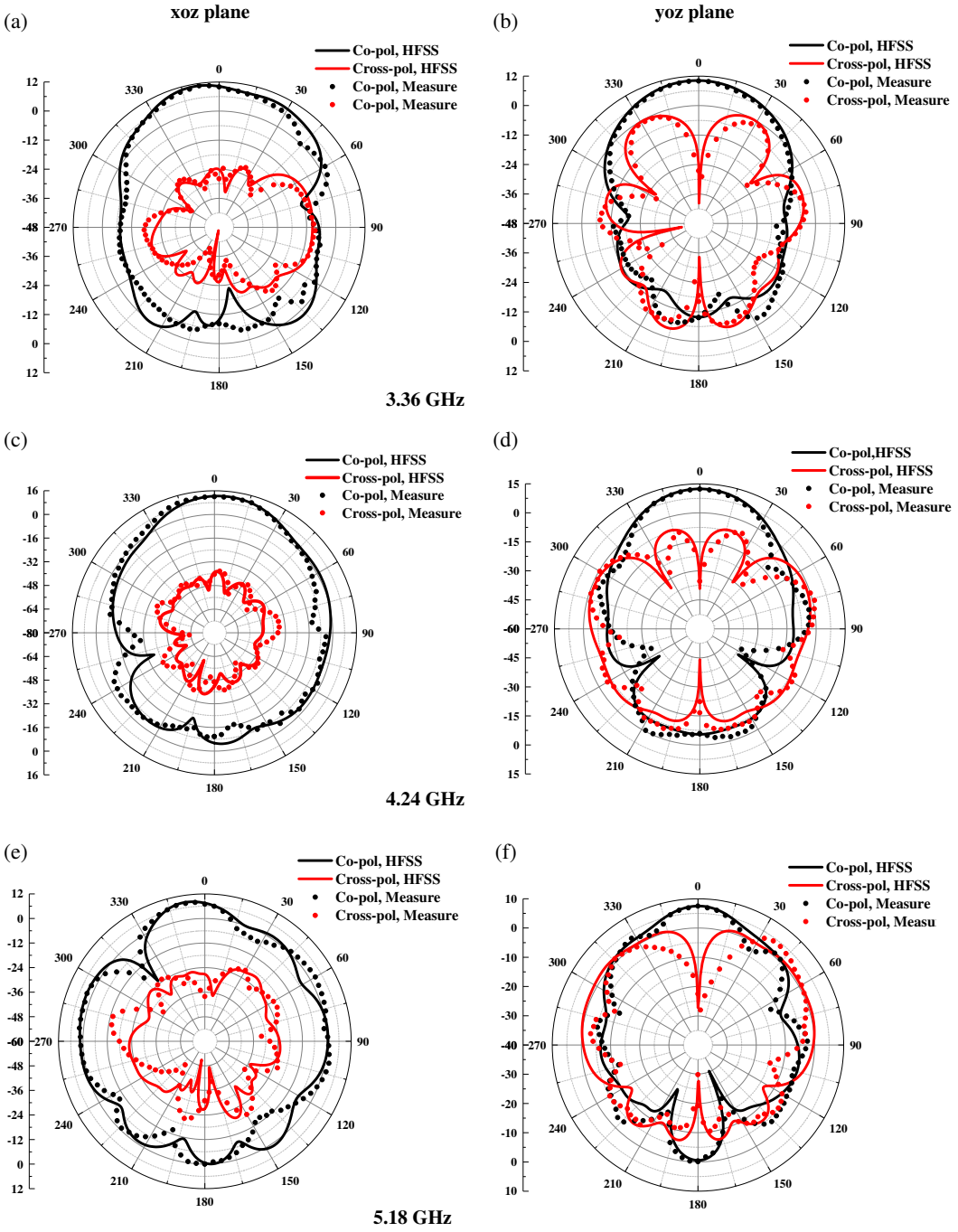

FIGURE 10. Radiation patterns of the proposed antenna. (a) xoz plane, 3.36 GHz. (b) yoz plane, 3.36 GHz. (c) xoz plane, 4.24 GHz. (d) yoz plane, 4.24 GHz. (e) xoz plane, 5.18 GHz. (f) yoz plane, 5.18 GHz.

impedance bandwidth of the antenna is not reduced, and the measured bandwidth is in the range of 2.84 GHz to 5.36 GHz. In addition, errors may be caused by losses in the SMA connector and transmission line or by the test environment.

3.2. Radiation Properties

The measured and simulated radiation patterns for the antenna working at 3.36 GHz, 4.24 GHz, and 5.18 GHz are shown in Figure 10. There is a clear contrast between the main and cross-polarization phenomena under the radiation direction diagrams for the E-plane and H-plane of the antenna. It can be noticed from Figure 10 that the main polarization is much better than the cross-polarization, and the antenna has good cross-polarization characteristics over the whole frequency range. In addition, the direction of maximum radiation in the main polarization direction map is basically distributed at a range of 330–30 degrees. At a frequency of 3.36 GHz, the cross-polarization level of the E-plane is about -10 dB, and that of the H-plane is about 0 dB. At a frequency of 4.24 GHz, the cross-polarization level of the E-plane is about -39 dB, and that of the H-plane is about 0 dB.

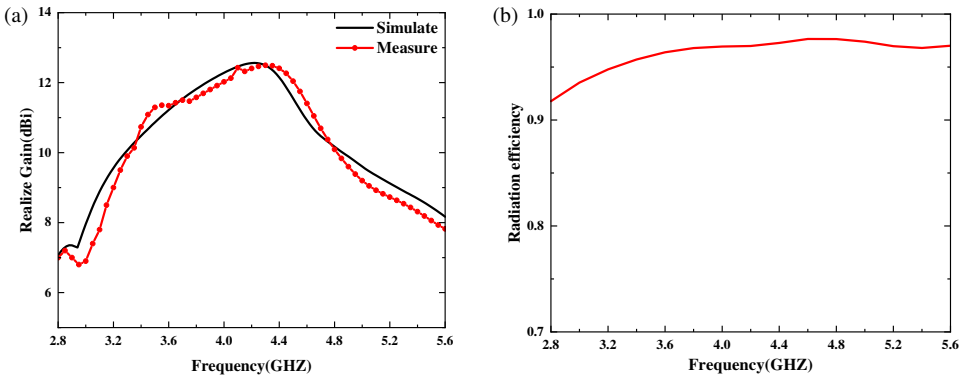

FIGURE 11. The proposed antenna: (a) peak gain and (b) radiation efficiency.

TABLE 2. Performance comparison of the proposed antenna with other works.

Ref.	size (mm^3)	Operating frequency (GHz)	FBW (%)	Peak gain (dBi)	Average gain (dBi)
[12]	137.5×95×8.4	3.9–5.9	40.8	11.1	\
[17]	106×100×25	3.27–5.15	45	12.2	10.04
[20]	70×40×2	5.13–5.85	13.2	9.7	\
[21]	120×70×1.6	1.8–2.5	32	12.1	\
[22]	260×162×21.6	1.45–2.55	55	12.3	\
[23]	160×66×20.08	3.5–5.8	51.12	12.4	\
This work	108×100×25	3.07–5.41	61.5	12.6	10.7

Below a frequency of 5.18 GHz, the cross-polarization level of the E-plane is about -12 dB, and that of the H-plane is about 0 dB.

Figure 11 shows the results of the peak gain and radiation efficiency of the antenna in the operating band. From Figure 11(a), the measured gain of the antenna basically agrees with the simulated gain. In addition, the antenna has a high radiation efficiency in the frequency band, which exceeds 90%.

3.3. Comparative Study

The proposed high-gain broadband antenna is comprehensively compared with several previously reported antennas in Table 2 in terms of size, operating bandwidth, and peak gain. The proposed antenna has a higher peak gain with a wider operating bandwidth at about the same size or smaller size than other works in the reference. Although the antenna in [20] has a smaller size, the bandwidth and peak gain in this paper are significantly larger than it. Moreover, the antenna proposed in this paper has a simpler geometry.

4. CONCLUSION

In this paper, a new high-gain, broadband microstrip patch antenna with dimensions of 108 mm×100 mm×25 mm is designed. The peak gain of the antenna is improved by folding the base plate structure parallel to the non-radiating edge. The suspended radiating patch is fed through a capacitive feed strip, which in turn is connected to a long-pin SMA connector. By optimizing the shape of the capacitive feed strip and the radiating unit, the impedance of the antenna is better matched, ultimately producing a 55% impedance bandwidth. During the optimization analysis, it was found that the current density on the diamond-shaped radiating patch was stronger than that on the rectangular radiating patch for the same excitation and that the radiation produced by the current on the folded floor was in phase. These changes favor the improvement of the bandwidth of the antenna as well as its radiation performance over the entire frequency range. The fabricated antenna has a measured peak gain of 12.6 dBi at 4.2 GHz and a measured bandwidth of 2.84 GHz to 5.36 GHz, which is an increase in bandwidth of about 1 GHz and an increase in gain of 3.3 dBi compared to the bandwidth of the initial antenna. This antenna can be used for 5G communications as well as broadband microwave imaging applications.

ACKNOWLEDGEMENT

This work was supported by the Graduate Innovation Fund of Anhui University of Science and Technology under grant No. 2024cx2063.

REFERENCES

[1] Lee, K.-F. and K.-F. Tong, "Microstrip patch antennas — Basic characteristics and some recent advances," *Proceedings of the IEEE*, Vol. 100, No. 7, 2169–2180, 2012.

[2] Wang, Z.-G., W. Ren, W.-Y. Nie, W. Mu, and C. Li, "Design of three-band two-port MIMO antenna for 5G and future 6G applications based on fence-shaped decoupling structure," *Progress In Electromagnetics Research C*, Vol. 134, 249–262, 2023.

[3] Chien, T.-F., H.-C. Yang, C.-M. Cheng, and C.-H. Luo, "Develop CPW-FED monopole broadband implantable antennas on the high dielectric constant ceramic substrates," *Microwave and Optical Technology Letters*, Vol. 52, No. 9, 2136–2139, 2010.

[4] Deshmukh, A. A. and K. P. Ray, "Broadband proximity-fed modified rectangular microstrip antennas," *IEEE Antennas and Propagation Magazine*, Vol. 53, No. 5, 41–56, 2011.

[5] Matin, M. A., B. S. Sharif, and C. C. Tsimenidis, "Broadband stacked microstrip antennas with different radiating patch," *Wireless Personal Communications*, Vol. 56, 637–648, 2011.

[6] Shao, Z., L.-F. Qiu, and Y. P. Zhang, "Design of wideband differentially fed multilayer stacked patch antennas based on bat algorithm," *IEEE Antennas and Wireless Propagation Letters*, Vol. 19, No. 7, 1172–1176, 2020.

[7] Fan, T.-Q., B. Jiang, R. Liu, J. Xiu, Y. Lin, and H. Xu, "A novel double U-slot microstrip patch antenna design for low-profile and broad bandwidth applications," *IEEE Transactions on Antennas and Propagation*, Vol. 70, No. 4, 2543–2549, 2022.

[8] Ding, Z., H. Wang, S. Tao, D. Zhang, C. Ma, and Y. Zhong, "A novel broadband monopole antenna with T-slot, CB-CPW, parasitic stripe and heart-shaped slice for 5G applications," *Sensors*, Vol. 20, No. 24, 7002, 2020.

[9] Kim, S.-W., H.-G. Yu, and D.-Y. Choi, "Analysis of patch antenna with broadband using octagon parasitic patch," *Sensors*, Vol. 21, No. 14, 4908, 2021.

[10] Mondal, K., "A novel-shaped reduced size FSS-based broadband high gain microstrip patch antenna for WiMAX/WLAN/ISM/X-band applications," *Journal of Circuits, Systems and Computers*, Vol. 30, No. 16, 2150290, 2021.

[11] Nguyen, D. D. and C. Seo, "A wideband high gain trapezoidal monopole antenna backed by frequency selective surface," *Microwave and Optical Technology Letters*, Vol. 63, No. 9, 2392–2399, 2021.

[12] Wang, R., Y. Duan, Y. Song, W.-G. Zhao, Y.-H. Lv, M.-S. Liang, and B.-Z. Wang, "Broadband high-gain empty SIW cavity-backed slot antenna," *IEEE Antennas and Wireless Propagation Letters*, Vol. 20, No. 10, 2073–2077, 2021.

[13] Xu, H., Z. Liang, Y. Li, K. Wang, Q. Cao, and Y. Long, "A high-gain microstrip magnetic dipole antenna utilizing slot-loaded high-order mode for WLAN applications," *IEEE Transactions on Antennas and Propagation*, Vol. 70, No. 10, 9130–9138, 2022.

[14] Cao, Y., Y. Cai, W. Cao, B. Xi, Z. Qian, T. Wu, and L. Zhu, "Broadband and high-gain microstrip patch antenna loaded with parasitic mushroom-type structure," *IEEE Antennas and Wireless Propagation Letters*, Vol. 18, No. 7, 1405–1409, 2019.

[15] Han, B. and S. Wang, "Design of ultra-wideband patch antenna based on folding-strip-shaped metamaterial concepts," *Journal of Nanoelectronics and Optoelectronics*, Vol. 17, No. 6, 939–945, 2022.

[16] Liu, K., D. Sun, T. Su, X. Zheng, and C. Li, "Design of flexible multi-band miniature antenna based on minkowski fractal structure and folding technique for miniature wireless transmission system," *Electronics*, Vol. 12, No. 14, 3059, 2023.

[17] Dhaundia, G. and K. J. Vinoy, "A high-gain wideband microstrip patch antenna with folded ground walls," *IEEE Antennas and Wireless Propagation Letters*, Vol. 22, No. 2, 377–381, 2023.

[18] Kasabegoudar, V. G. and K. Vinoy, "A broadband suspended microstrip antenna for circular polarization," *Progress In Electromagnetics Research*, Vol. 90, 353–368, 2009.

[19] Kasabegoudar, V. G. and K. J. Vinoy, "Coplanar capacitively coupled probe fed microstrip antennas for wideband applications," *IEEE Transactions on Antennas and Propagation*, Vol. 58, No. 10, 3131–3138, 2010.

[20] Wang, Z., J. Liu, and Y. Long, "A simple wide-bandwidth and high-gain microstrip patch antenna with both sides shorted," *IEEE Antennas and Wireless Propagation Letters*, Vol. 18, No. 6, 1144–1148, 2019.

[21] Malaisamy, K., G. Haridoss, J. A. Pandian, and S. K. Rima, "Design of crossed dipole Yagi-Uda MIMO antenna for radar applications," *International Journal of Antennas and Propagation*, Vol. 2022, No. 1, 8157541, 2022.

[22] Chopra, R. and G. Kumar, "Broadband and high gain multilayer multiresonator elliptical microstrip antenna," *IET Microwaves, Antennas & Propagation*, Vol. 14, No. 8, 821–829, 2020.

[23] Alwareth, H., I. M. Ibrahim, Z. Zakaria, A. J. A. Al-Gburi, S. Ahmed, and Z. A. Nasser, "A wideband high-gain microstrip array antenna integrated with frequency-selective surface for Sub-6 GHz 5G applications," *Micromachines*, Vol. 13, No. 8, 1215, 2022.